Electrochimica Acta 492 (2024) 144386

Contents lists available at ScienceDirect

Electrochimica Acta

journal homepage: www.journals.elsevier.com/electrochimica-acta

Probing iodide/iodonium salt interactions with single-walled carbon nanotubes for resilient electrochemical capacitor

Maciej Tobis [a], Justyna Piwek [a], Anetta Płatek-Mielczarek [a], Łukasz Przypis [b], Dawid Janas [b,*], Elżbieta Frąckowiak [a,*]

[a] Institute of Chemistry and Technical Electrochemistry, Poznan University of Technology, Poznan, Poland
[b] Faculty of Chemistry, Silesian University of Technology, Gliwice, Poland

ARTICLE INFO

Keywords:
Single-walled carbon nanotubes
Electrochemical capacitors
Iodonium salt
Iodide
Activated carbon

ABSTRACT

Self-standing films from single-walled carbon nanotubes (SWCNTs) were successfully used as electrochemical capacitors' (ECs) electrode material, which exhibited state-of-the-art characteristics. The surface of SWCNTs was modified by iodonium salt molecules that substantially and permanently improved their electrical conductivity. The addition of pyridinium iodine chloride salt (IPyCl) quadrupled the value of the electrical conductivity of the SWCNT film, which reached values as high as 1022 S cm^{-1}. Subsequently, the electrochemical performance of the newly designed self-standing SWCNTs with deposited IPyCl in aqueous neutral 1 M Li_2SO_4 and redox-active 1 M KI electrolytes was thoroughly analysed. Because redox activity of iodine species was observed mainly on the positive electrode, activated carbon with a developed surface area was used as a negative electrode to balance the faradaic charge. Due to the notable stability of iodonium salt dopant (instead of labile halogen-containing compounds typically used for SWCNT doping), robust charge/discharge performance of EC was demonstrated (> 10 000 cycles) in Li_2SO_4 electrolyte. Moreover, a significant improvement of capacitor metrics (from 49 to 75 F g^{-1}) was obtained when electrodes modified by previously unexplored iodonium salt were utilized in 1 M KI electrolyte. Extensive analysis of the obtained data led to the elucidation of the doping mechanism responsible for the aforementioned achievements. The novel SWCNT-based electrodes enhanced with iodonium salt are auspicious materials, which can be used to build EC systems of appreciable capacitance.

1. Introduction

Electrochemical capacitors (ECs) are emerging high-power electrical energy storage systems able to deliver the accumulated charge within seconds rapidly [1–4]. Amongst different energy devices, they fill an important niche between the conventional capacitors and lithium-ion batteries on the Ragone plot [5]. The principal mechanism of EC charge storage is based on the formation of electrical double-layer (EDL) upon polarization of the electrodes and consequent diffusion of ions towards oppositely charged surfaces [6]. Purely physical nature of ion attraction allows the device to reach usually higher values of power density than batteries. At the same time, ECs possess higher values of energy density than conventional capacitors mostly due to well-developed specific surface area (SSA) of electrodes. There are many electrode materials that were already tested in EC systems, e.g., transition metal dichalcogenides [7], conductive polymers [8,9], and oxides [10,11] due to their high capacitance originating from pseudocapacitive effects. However, the majority is still based on carbonaceous materials due to their wide abundance, structural diversity, and usually high electrical conductivity [12,13].

Ideally, the ECs electrode material should be characterized by well-developed SSA, wide pore size distribution (PSD), and high electrical conductivity [14–16]. Carbonaceous materials, e.g., activated carbons (ACs), carbon nanotubes (CNTs), or carbon blacks, meet these criteria and are able to provide high capacitance at high charge/discharge rates [17]. CNTs are particularly attractive materials within energy storage devices owing to their ballistic electrical conductivity, especially needed for superior charge/discharge power rates [18–20] and the possibility of zero-resistance electron transfer [21]. To further enhance the capacitance of CNT-based electrode material, one may incorporate redox-active components at the electrode/electrolyte interface to increase the amount of charge stored in the form of reversible redox reactions. It has already been demonstrated that the use of halogen salts (e.g., iodides or bromides) as an additive to the electrolyte improves the

* Corresponding authors.
E-mail addresses: dawid.janas@polsl.pl (D. Janas), elzbieta.frackowiak@put.poznan.pl (E. Frąckowiak).

https://doi.org/10.1016/j.electacta.2024.144386
Received 27 December 2023; Received in revised form 17 April 2024; Accepted 2 May 2024
Available online 4 May 2024

overall performance of the ECs by exhibiting reversible faradaic reactions [22,23]. The following redox reaction is responsible for the battery-like electrochemical behaviour of positive electrode in system containing iodides dissolved in electrolyte [23] (1):

$$2I^- \leftrightarrow I_2 + 2e^- \quad (1)$$

Thanks to this reaction, iodine can exhibit high capacity of 211 mAh g^{-1}, which is a competitive alternative to other pseudocapacitive materials [24]. When I_2 is dissolved in iodide solution it is also possible to form polyiodides, i.e., I_3^- and I_5^- (2–3) when the electrode is cycled over long time. Depending on the pH of electrolyte solution, it is also possible to create IO_3^- (4) according to the reaction below [25]:

$$I^- + I_2 \leftrightarrow I_3^- \quad (2)$$

$$2I_3^- + I_2 \leftrightarrow I_5^- \quad (3)$$

$$I^- + 3H_2O \leftrightarrow IO_3^- + 6H^+ + 6e^- \quad (4)$$

Alkali metal iodides show dependency of the electrode capacitance from cation properties, e.g., diffusion coefficient and ion mobility. In consequence, positive electrode in aqueous solution of rubidium iodide (RbI), which has perfectly aligned cation-to-anion and cation-to-solvent properties presented the highest capacitance of 2272 F g^{-1} [26]. Unfortunately, such enormous capacitance was found in the 50 mV range of potential. Iodides are not only attractive due to their supplementary redox reactions, but also due to their environmental friendliness, high abundance, and notable electrical conductivity (up to 275 mS cm^{-1} for 2 M NaI) [27]. Usually, iodides are employed together with high specific surface area carbonaceous material due to their porous network to reversibly host iodine/iodides ions and immobilize their polyiodide forms (I_3^- and I_5^-) [28,29]. Apart from iodides in electrolyte, it is possible to incorporate iodine on the surface of carbonaceous materials through heat or plasma treatment to improve its electrical conductivity and introduce supplementary redox reactions [30,31]. Unfortunately, iodine is prone to sublimation, which may affect the stability of the iodised material.

In this article, we present how a non-volatile iodine-containing alternative can solve this problem. Self-standing films from single-walled carbon nanotubes (SWCNTs) were doped with in-house made iodonium salt (pyridine iodine monochloride – IPyCl or denoted as I), which greatly improved its electrical conductivity. Subsequently, these novel materials were subjected to a thorough electrochemical characterization to gauge their utility for capacitor application. Because of the limited solubility of IPyCl in water and much lower vapour pressure, compared with typical halogen-containing SWCNT dopants, the favourable doping effect was stable. As a result, the as-made electrodes displayed superior and, most importantly, steady performance in time.

2. Experimental

2.1. Material preparation

SWCNT films (CNTs) were prepared from high-quality SWCNTs (Tuball, OCSiAl, diameter: 1.6 ± 0.4 nm). In brief, 60 mg of SWCNTs were introduced to 20 mL of toluene, and the mixture was sonicated over ice for 15 min (UP200St sonicator) until a homogeneous SWCNT dispersion was reached. Then, it was vacuum filtrated using PTFE membranes (pore size: 0.22 μm, diameter: 47 mm) to obtain SWCNT films. Finally, the films were delaminated from the membrane and dried thoroughly to eliminate the influence of the solvent on the properties.

IPyCl (denoted as I) was synthesized using the following approach. A solution of iodine monochloride (19 g) in acetic acid was added slowly at 0 °C with continuous stirring to a solution of pyridine (7.5 g) in acetic acid. The progress of reaction was checked by thin-layer chromatography (TLC). The reaction was finished when the precursor was no longer detectable. The obtained pale-yellow solid was filtered, dried and recrystallized in ethyl alcohol.; m.p. 121–123 °C; 1H NMR (600 MHz, CD_3CN) δ *^1H NMR* (600 MHz, CD_3CN) δ 7.55 – 7.48 (m, 2H), 8.09 (t, J = 7.5 Hz, 1H), 8.70 (d, J = 4.8 Hz, 2H); *^{13}C NMR* (151 MHz, CD_3CN) δ 128.08, 141.58, 149.61 (Fig. S1 and S2).

2.2. Doping of CNT films

Prepared CNT films electrodes (ca. 10 mg) were later soaked with iodonium salt solution (2.5 mg dissolved in 5 mL of methanol) and left for solvent evaporation. Such prepared electrodes were later dried in 70 °C overnight. After drying, doped electrodes were weighed, which allowed for the determination of iodonium salt loading.

2.3. Materials characterization

Raman spectra were recorded on pristine and doped electrode materials (Fig. S1) by using Thermo Scientific DXR Raman Microscope with a laser emitting at 532 nm and a power of 6 mW. Spectra are average of three measurements, each lasting 10 s. The deconvolution of spectra was performed employing Lorentzian peak fitting.

^1H and ^{13}C NMR spectra (Figs. S2, 3) were recorded at 298 K on a Varian System 600 MHz (600 MHz for ^1H and at 150.8 MHz for ^{13}C). Spectra were calibrated relative to CH_3CN residual proton and carbon chemical shifts: (δ = 1.94 ppm for ^1H NMR and δ = 1.39 ppm for ^{13}C NMR). Coupling constants (J) are reported in Hertz (Hz). The multiplicity of the signals is given as d (doublet), t (triplet), m (multiplet).

A thermogravimetric analyser (TGA, Mettler Toledo TGA/DSC 1 STA) gauged the thermal stability of CNTs. The samples were heated in a flow of air (20 mL min^{-1}) with a heating rate of 10 °C min^{-1} from 25 °C to 1000 °C.

The material textural properties were evaluated through N_2 sorption at 77 K. The isotherms of adsorption/desorption were recorded with the use of ASAP 2460 (Micromeritics, USA). The materials were degassed in a flow of helium at 100 °C for 24 h. Prior the nitrogen adsorption, the samples were degassed for 5 h in a vacuum. The specific surface area (SSA) was calculated by Brunauer-Emmett-Teller (BET) model using 0.01 to 0.05 P/P_0 range. The pore size distribution (PSD) was evaluated with the use of SAIEUS program (Micromeritics, USA) with a 2D-NLDFT heterogenous surface model.

The electrical conductivity of CNT films before and after doping was studied using the 4-probe approach. A source metre (Keithley 2450) delivered low current (10 mA) to the specimens (10 mm x 20 mm) to ensure that the samples were not subjected to Joule heating. Measured conductance values were recalculated to conductivity by considering samples' thickness determined with an electronic micrometer.

For electrochemical measurements, electrodes of a 10 mm diameter were cut from binder-free pristine CNTs, CNTs∘I films and activated carbon tissue (KYNOL 507–20, Kynol GmbH). Symmetric and asymmetric Swagelok® cells with (Hg/Hg_2SO_4, E_0=640 mV vs. SHE) reference electrode were employed for electrochemical tests. Each configuration contained two electrodes separated with glass fibre membrane (Whatman, GF/A® 260 μm thick and 12 mm diameter) soaked with ca. 150 μL of electrolyte. Systems were employing different electrolytes, i.e., 1 M Li_2SO_4 and 1 M KI. Electrochemical behaviour of the cells was evaluated by using cyclic voltammetry with scan rate of 1 to 200 mV s^{-1}, galvanostatic charge/discharge from 0.1 A g^{-1} to 2 A g^{-1} and impedance spectroscopy at 0 V in the 1 mHz to 100 kHz frequency range. Initially systems were tested within 0 – 0.8 V voltage range. After that, they were subjected to voltage extension from 0.8 – 1.5 V. All electrochemical results are expressed per cell, i.e., mass of both electrodes was considered during calculations. Calculation methodology is described below (Eqs. (5)–(9)).

2.4. Calculation of gravimetric capacitance of the cell

Following formulas were used for calculation the capacitances from

cyclic voltammetry, galvanostatic charge/discharge and electrochemical impedance spectroscopy:

$$C_{CV} = \frac{I}{\frac{dU}{dt} \cdot m} \tag{5}$$

$$C_{GC/D} = \frac{2 \cdot I \cdot A}{U^2 \cdot m} \tag{6}$$

$$C_{EIS} = \frac{1}{\pi \cdot f \cdot |z| \cdot m} \tag{7}$$

$$E = \frac{C_{GC/D} U^2}{7200} \tag{8}$$

$$P = \frac{E}{t_{dis}} \tag{9}$$

where, C_{CV}: cell capacitance calculated from cyclic voltammetry (F g^{-1}), $C_{GC/D}$: cell capacitance calculated from galvanostatic charge/discharge (F g^{-1}), I: current (A), dU/dt: scan rate (V s^{-1}), m: mass of positive and negative electrode (g), A: area under discharge curve (V s), U: voltage (V), f: frequency (s^{-1}), z: resistance (Ohm), E: energy (Wh g^{-1}), P: power (W g^{-1}), t_{dis}: cell discharge time (h).

3. Results and discussion

3.1. Physicochemical characterization

The preparation of single-walled carbon nanotube (CNT) films is presented in Fig. 1. Sonication employed for the individualization of CNTs may introduce defects into the structure [32], so it was essential to verify that the high crystallinity of the raw material was preserved. Initial characterization by TGA and TEM revealed indirectly that the CNTs have exceptional purity, so the processing did not damage the material. Firstly, the thermogram indicated temperature stability against oxidation up to ca. 400 °C, which is a remarkable result for single-walled CNTs even if one could expect a much lower onset of thermal degradation [33]. Secondly, imaging of the CNTs by TEM displayed that the material was essentially contamination-free. Besides that, it was observed that CNTs were arranged into thick bundles, which should reduce junction resistance between CNTs [34], thereby making

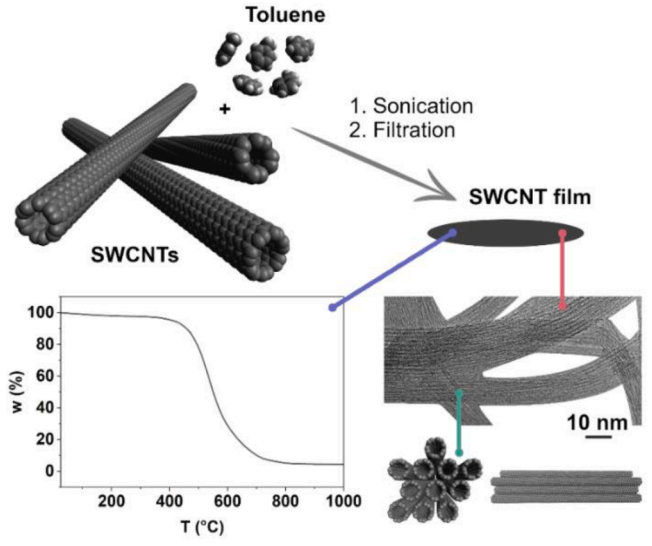

Fig. 1. Manufacture method of single-walled CNT films used in the study and their characterization by TGA and TEM (background removed). The network comprises CNT bundles, schematically shown in the bottom right corner, which promotes charge propagation.

these CNT films highly suitable for electrochemical applications.

To validate this hypothesis, the electrical conductivity of the nanocarbon material was examined by the 4-probe approach (Fig. 2A). The as-made CNT films had an electrical conductivity of 251±12 S cm^{-1}, which is a good value for unmodified CNT ensembles [35]. Interestingly, the incorporation of pyridine iodine monochloride (IPyCl) into the CNT network quadrupled the electrical conductivity, which, upon doping, reached 1022±18 S cm^{-1}. Thus, the addition of the examined iodonium salt was beneficial as it enhanced the electrical conductivity of CNTs due to the presence of chloride [32], nitrogen [36], and iodide [37] moieties, all of which have a favourable impact on the electrical properties of CNTs. We previously reported that interhalogen compounds such as iodine monochloride (ICl) increase the density of states in metallic CNTs and decrease the bandgap in semiconducting CNTs, which makes the material more conducting [37]. In addition to these phenomena, the employed dopant contains pyridinium cation, which may further dope the CNTs. In the case of this study, the amount of doped iodonium salt was 25 wt.% with respect to SWCNTs.

3.2. Evaluation of the material using Raman spectroscopy

The structure of the CNTs was further investigated by Raman spectroscopy (Fig. S3). High defect-sensitive I_G/I_D index exceeding 20, in both cases (before and after IPyCl doping), indicated uniform and immaculate structure. The defect-induced D peak was virtually nonexistent. The dominant Raman features of CNTs, i.e., G band at 1590 cm^{-1} and radial breathing mode (RBM) in the range of 125–200 cm^{-1} were subjected to more detailed analysis in Fig. 2B. Deconvolution of G band using Lorentzian line shape revealed the presence of two peaks associated with the nanotube cylinder flexure, G^+ and G^-. The emergence of G^+ mode was related to the vibrations of carbon atoms along the nanotube plane, while the G^- mode to the out-of-plane vibrations. The shape of these features is sensitive to the nature of CNTs, whether they are metallic or semiconducting [38]. Table S1 shows multiple-peak fitting parameters for deconvoluted spectra. After doping the CNTs with iodonium salt, we observed a slight change in the position of both modes. The distance between the modes decreased after doping with iodonium salt. It could result from the interaction between CNTs and iodine, confirming doping of the material. This and the evident change in the shape and position of the G mode [39,40] revealed that the CNTs became more metallic after the treatment.

The RBM itself is a bond-stretching out-of-plane phonon mode in which all carbon atoms move in the radial direction. The RBM frequency is inversely proportional to the tube diameter, quantifying the number of atoms along the circumferential plane [41]. The small but discernible difference in the shape and position of the RBMs for pristine (165 cm^{-1}) and modified (183 cm^{-1}) materials could be explained by the increased number of atoms, and consequently mass, moving in the circumferential plane after CNT doping [42]. It could also indicate the change of the chemical nature of the CNTs upon doping with iodonium salt molecules [43]. Halogens are also observable by the Raman spectroscopy, but their unstable nature impedes accurate data interpretation. In the case of iodine, the I^- ion appears in the region of 190–170 cm^{-1} in the form of a broad band. Considering CNTs, both spectra are covered by RBM in the I^- ion range. At 110 cm^{-1} Raman shift, we could observe a narrow peak, which could be attributed to the formation of iodide species such as I_3^- [27,44]. The presence of such peak could be related to the possible disproportionation of ICl leading to the generation of polyiodide compounds such as I_3Cl [45]. This hypothesis is supported by the type of liquid medium in which the experiments were conducted. Methanol is hygroscopic, and the presence of moisture may partly promote the formation of elemental iodine from iodine monochloride due to hydrolysis [46]. Consequently, as-obtained iodine may react with iodide anions present in IPyCl to synthesize polyiodide species, according to the equations given in the introduction section. Moreover, the relatively broad interhalogen I-Cl stretching band emerged with its maximum

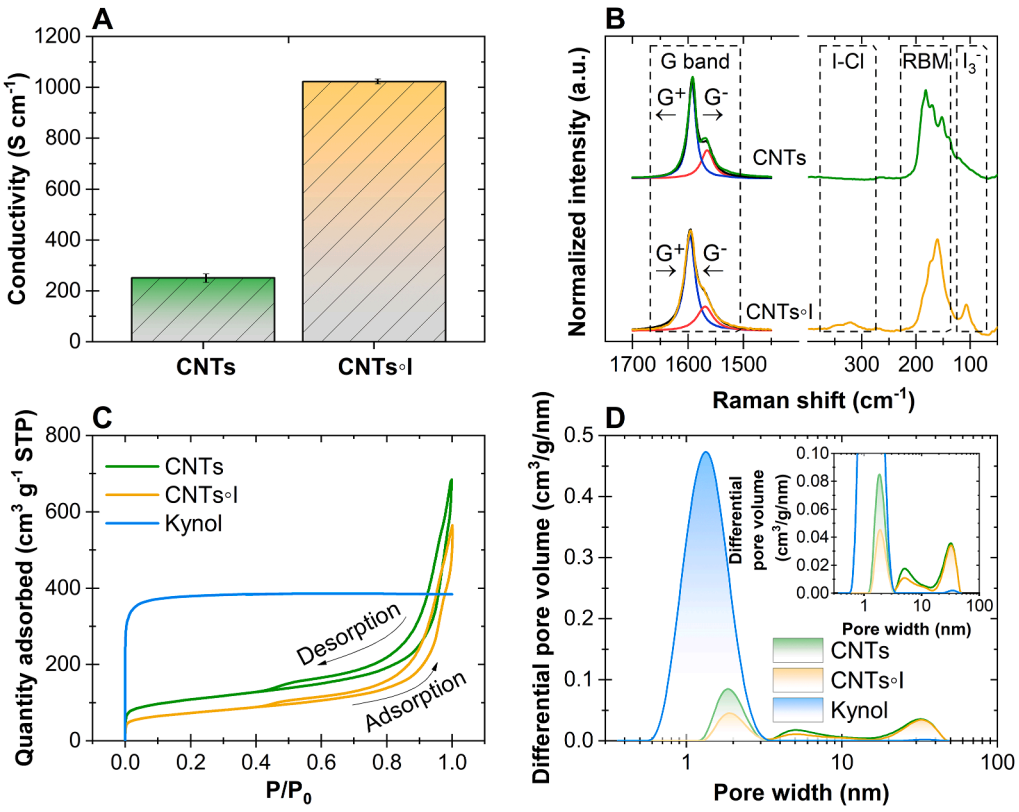

Fig. 2. A) Electrical conductivity of single-walled CNTs before and after doping with iodonium salt (IPyCl), B) Dominant Raman features for pristine CNTs and CNTs◦I with marked characteristic high-energy modes of G^+ and G^- indicating change in the nature of the CNTs after doping with iodonium salts, C) N_2 sorption isotherm of pristine single-walled CNTs, CNTs◦I and Kynol, D) Pore size distribution.

centred at ca. 325 cm^{-1} [44]. The position of this peak is typically very much solvent-dependent. The wavenumber range in which it was registered herein for methanol matched the position of this peak for other solvents of similar characteristics reported in the literature.

3.3. *Nitrogen sorption at 77 K*

The nitrogen sorption isotherms of the CNTs, CNTs◦I and activated carbon cloth (Kynol® 507–20) are presented in Fig. 2C with the porosity results summarized in Table 1. Both CNT samples displayed isotherm type II associated with nonporous or mesoporous materials. CNTs are usually entangled, forming the mesoporous network. Oppositely, carbon cloth exhibited isotherm type I with strict microporous texture. In the case of CNTs, at low relative pressure, isotherms showed a sharp knee, indicating the formation of N_2 monolayer, which was quickly filled, proving low content of micropores in the case of CNTs and CNTs◦I. Accordingly, the multilayer was formed and gradually increased up to the P/P_0=1, indicating a high content of mesopores. During desorption, hysteresis type 3 was observed indicating cavitation process at the intersection of the adsorption/desorption isotherm [47].

The CNT film showed high specific surface area of 380 $m^2\ g^{-1}$, which was in good agreement with literature values for single-walled CNTs [48,49]. After the deposition of iodonium salt, one could observe a decrease of SSA to 250 $m^2\ g^{-1}$, which corresponded to blocking ca. 30% of available surface area. This was not simply an effect of the dopant introduction, which should lower the SSA only to 304 $m^2\ g^{-1}$ at the chosen IPyCl content. Fig. 2D shows pore size distribution for pristine and modified materials. One major peak within the range of micro- and mesopores could be differentiated (from 1 to 3 nm). Additionally, a large diversity of mesopores could be observed (from 3 to 50 nm). Based on the DFT calculation, one could detect a major decrease in the micropore volume, which proves that the iodonium salt has been mainly distributed in the micropores. Considering this, the intact mesoporous texture of CNTs could provide excellent routes for ions transport during charge/discharge processes. On the contrary, carbon cloth showed mainly microporous structure with a small content of mesopores. Naturally, it revealed the highest SSA equal to 1520 $m^2\ g^{-1}$.

Table 1
Porous texture properties of CNTs, CNTs◦I and Kynol.

Sample	SSA [$m^2\ g^{-1}$]	V_{MICRO} [$cm^3\ g^{-1}$]	V_{MESO} [$cm^3\ g^{-1}$]	$L_{0\ MICRO}$ [nm]	$L_{0\ MESO}$ [nm]
CNTs	380	0.04	0.78	1.71	15.09
CNTs◦I	250	0.02	0.68	1.73	17.63
Kynol	1520	0.45	0.10	1.30	2.96

3.4. *Scanning electron microscopy*

SEM analysis was carried out to investigate changes in the microstructure resulting from doping the CNTs (Fig. 3). The unmodified material was clearly porous, with CNTs and CNT bundles arranged in an isotropic fashion, as expected from a CNT ensemble made by filtration. However, upon doping the material with IPyCl, a substantial increase in the packing density was observed. Consequently, the surface area was reduced. Reorientation of the CNTs is another factor that contributed positively to the observed increase in the electrical conductivity of the CNT films after the processing. Besides previously discussed electronic effects caused by doping, shorter distance between individual CNTs also promoted the transport of charge carriers through the CNT network.

3.5. *Electrochemical behaviour*

Initially, three different symmetrical and asymmetrical Swagelok® setups consisting of CNTs and CNTs◦I have been constructed to observe

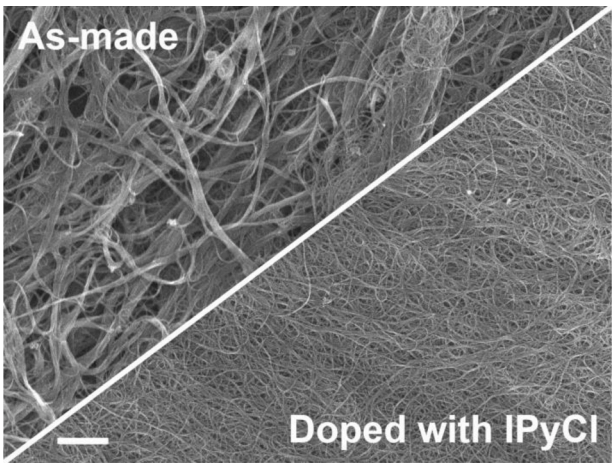

Fig. 3. SEM micrographs of CNT films before and after doping with iodonium salt.
The scale bar is 10 μm.

the influence of iodonium salt addition on electrochemical performance in 1 M Li_2SO_4 electrolyte (Fig. 4). It should be noted that the values of specific capacitance were calculated per cell (Equations 1–5). The values of capacitance calculated per electrode would be four times higher than per cell. Unsurprisingly, symmetrical cell (-) CNTs ‖ CNTs (+) (Fig. 4A, B) showed rectangular cyclic voltammogram (CV) shape and isosceles galvanostatic charge/discharge (GC/GD) curves, which was the result of high material conductivity and purely capacitive charge storage mechanism. The system showed very low internal equivalent series resistance (ESR) of 0.4 Ohm, which resulted in high charge propagation (Fig. 4E, F). Despite high conductivity, the cell also exhibited the smallest specific capacitance of 6 F g^{-1} at 0.1 A g^{-1} (Fig. 4E, F). When doped CNTs were employed as a positive electrode in the system (-) CNTs ‖ CNTs∘I (+), a considerable difference can be spotted in the electrochemical behaviour of the cell. We have also performed studies of depositing different content of iodonium salt on the surface of CNTs (Fig. S4). The content varied from 0 wt.% (pure CNTs) to 50 wt.%. As one can see, low coulombic efficiency was obtained for 50 wt.% of added salt. Therefore, for further studies, 25 wt.% of iodonium salt was selected as the highest content giving rise in capacitance boost, but still maintaining high enough charging/discharging efficiency. Based on the CV (Fig. 4A), one could observe an improvement of the overall specific capacitance with a small broad reversible hump in the range of 0 – 0.4 V, associated with the iodonium salt surface redox reaction. Surprisingly, the capacitance was higher in a whole voltage range, not only within the redox activity area (0 – 0.4 V), suggesting that the redox reaction on positive electrode affects the whole EC voltage range. Accordingly, this system exhibited improved specific capacitance of 10 F g^{-1} at 0.1 A g^{-1} (Fig. 4E, F) with a higher ESR value of 0.58 Ohm and lower charge propagation than a symmetrical cell (Fig. 4D). Increased ESR could be explained by the enhanced resistance at the electrode/electrolyte interface. Consequently, to balance the charges and fully exploit the redox processes on the positive electrode, we paired activated carbon cloth, which, thanks to the developed SSA, had a higher intrinsic capability to store charge than CNTs. Consequently, (-) Kynol ‖ CNTs∘I (+) system exhibited a two-fold capacitance increase in the whole voltage range. The redox reaction has been shifted towards higher voltage range of 0.5 – 0.8 V, presumably due to better charge distribution on positive and negative electrodes. The GC/GD profiles remained isosceles after electrode doping (Fig. 4B). The setup was able to reach a high specific capacitance of 20 F g^{-1} at 0.1 A g^{-1} (Fig. 4E, F) with slightly more elevated ESR of 0.88 Ohm than CNTs electrode-based system and intermediate charge propagation, most likely due to higher intrinsic resistance of activated carbon cloth electrode.

Iodides in the form of I^- ions employed as an electrolyte (e.g., 1 M KI) were the subject of the intensive studies due to very high capacitances (up to 300 – 400 F g^{-1}) [27]. However, the long-term performance of the cell with iodides was usually restricted due to the formation of polyiodides. It resulted in quick capacitance fade due to blockage of the porous texture of both electrodes [29,50]. The response to that issue, was the application of porous carbon as a positive electrode with matched porous texture to the iodide ions [51]. In our case, iodonium salt was in the solid form bonded to the surface of the CNTs, acting as redox species with a positive impact on the electrode conductivity. Following this, we studied the interaction between iodonium salt and iodide ions present in the electrolyte solution. We have assembled cell (-) Kynol ‖ CNTs∘I (+) in 1 M KI and compared it with the cell assembled in 1 M Li_2SO_4 (Fig. 5A, B).

The cell with 1 M KI showed a considerable increase of the specific capacitance mainly thanks to the iodide $2I^-/I_2$ redox reaction in the range of 0 – 0.2 V (Fig. 5A, B). For comparison, we assembled the cell with pristine CNTs as a working electrode (-) Kynol ‖ CNTs (+) in 1 M KI (Fig. S5). Capacitance has been significantly increased from 49 F g^{-1} to 75 F g^{-1} for cells without and with iodonium salt, respectively. It indicated beneficial interactions between iodide ions from electrolyte and deposited iodonium salt, especially on the positive electrode. As the energy of the system increased with the square of the voltage, we wanted to expand the operational voltage window of cells employing 1 M Li_2SO_4 and 1 M KI as electrolytes while monitoring the potential of each electrode (Fig. 5C–F). In both cells, electrodes operated near the potential of the theoretical hydrogen and oxygen evolution reaction after voltage extension to 1.5 V in 1 M Li_2SO_4 and in 1 M KI. Considering CV response, the operating voltage for KI solution was limited to 1.2 V and remained 1.5 V for lithium sulfate. High operational window of 1.5 V in the Li_2SO_4 was also proof of high purity and non-defected structure of the prepared CNT film. Nevertheless, there are no reports showing single-walled CNTs operating at such elevated voltages mostly due to oxidation of the positive electrode. Herein, the presence of iodonium salt could prevent the oxidation of the positive electrode. The potential of redox reaction was comparable for both systems (+0.3 to +0.6 V vs. SHE), meaning that the nature of the reaction could be the same. Interestingly, in iodonium salt, halogen atom acted as an electron acceptor, whereas pyridine played the role of donor. It was assumed that such compound did not tend to form polyiodides, resulting in a prolonged cycle life. The shuttling effect was decreased as well. The difference between the capacitance values of the positive electrode operating in 1 M Li_2SO_4 and 1 M KI indicated some electrochemical interaction between dissolved iodide ions from electrolyte and iodonium salt. Easily accessible iodonium salt within CNT texture could react with iodide ions, additionally boosting the specific capacitance. As can be observed in Fig. S6 (Pourbaix diagram) we can correlate the probability of occurring specific redox reactions at the electrode/electrolyte interface based on the potential and pH in the vicinity of iodonium salt. In the current experimental system iodide species are present, hence, mostly reaction (1), given in the introduction section, takes place. Obviously, formation of polyiodides should be considered during electrochemical reactions. Comparing electrochemical behaviour (Fig. 5) in the redox- (KI) and capacitive-electrolyte (Li_2SO_4), one can observe the same iodide activity on the positive electrode - as it is expected from the Pourbaix diagram ($I_2/2I^-$ redox pair). Taking into account the neutral pH in our system, the reaction (4) can be excluded.

Furthermore, we decided to evaluate the effect of scan rate and application of different current densities (Fig. 6). A gradual decrease of the capacitance of both cells was observed over increasing sweep rate with solely capacitive behaviour at 200 mV s^{-1}. The cell assembled with 1 M Li_2SO_4 showed 25 F g^{-1} (~100 F g^{-1} per electrode), and the cell with 1 M KI presented 68 F g^{-1} (~270 F g^{-1} per electrode) at 0.2 A g^{-1}. The cycle life of the cells was determined at 1 A g^{-1} current density (Fig. 7) with 20% of initial capacitance loss as an effective criterion of a capacitor end-of-life [52]. The cell with 1 M Li_2SO_4 showed a gradual

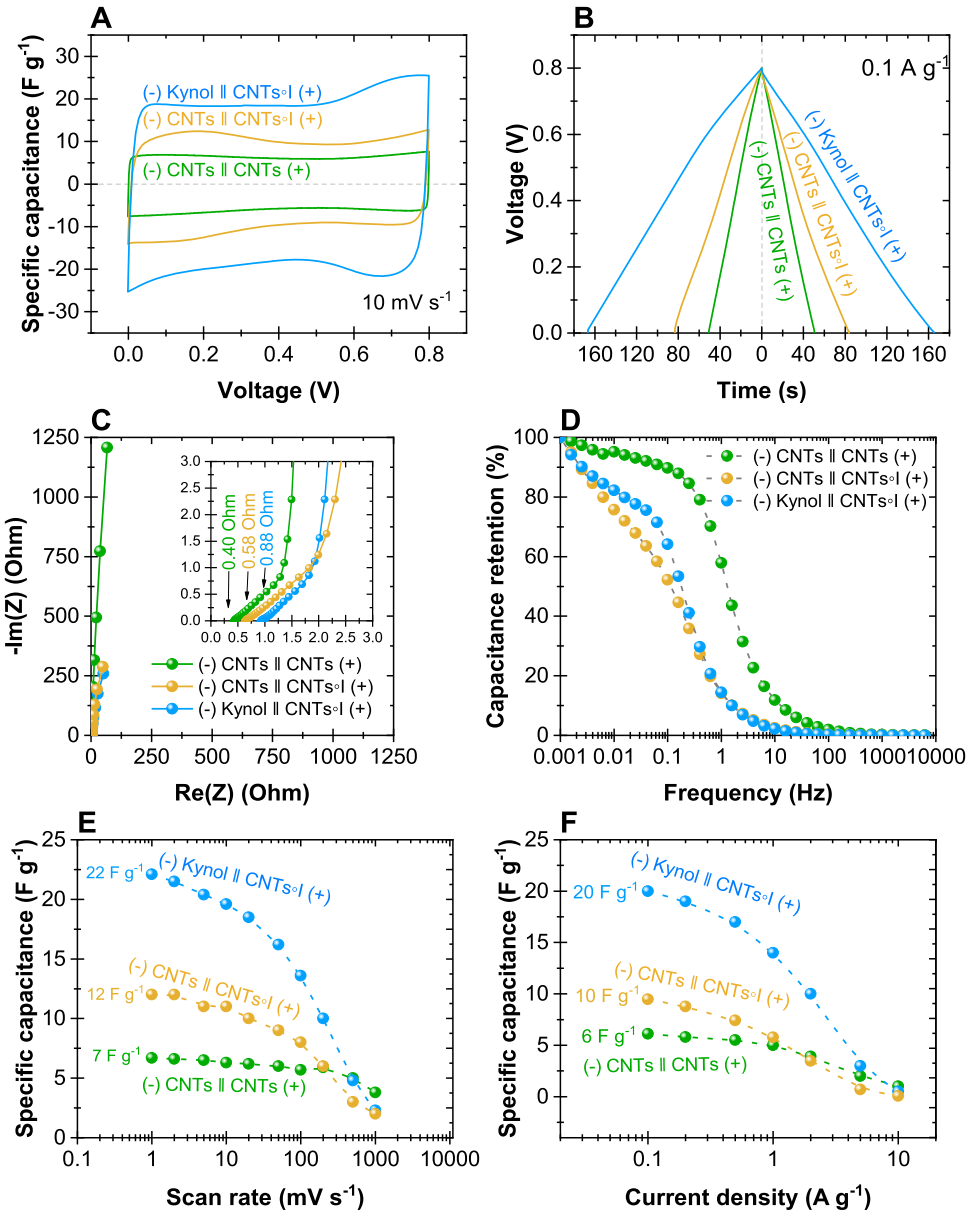

Fig. 4. Electrochemical characterization of cells assembled with 1 M Li_2SO_4 electrolyte, A) Cyclic voltammograms at 10 mV s^{-1}, B) Galvanostatic charge-discharge at 0.1 A g^{-1}, C) Electrochemical impedance spectroscopy recorded at 0 V, D) Specific cell capacitance retention vs. frequency, E) Specific cell capacitance vs. scan rate, F) Specific cell capacitance vs. current density.

decrease of the capacitance for up to 10 000 cycles. It could indicate that the deposited iodonium salt did not deteriorate the system. Selected profiles of the galvanostatic discharge showed typical isosceles shape. It was also surprising for the cell employing CNTs on the positive electrode to deliver stable long-term performance at as high voltage as 1.5 V. Usually, high voltage tests easily lead to oxidation of CNT surface, consequently limiting their maximum capacitance. It could mean that the iodonium salt did not only provide supplementary redox reactions but also protected the CNT surface from oxidation. The cell with 1 M KI (Fig. 7B) showed characteristic capacitance decay over time, leading to around 3000 efficient charge/discharge cycles until reaching 20% of initial capacitance loss. Typically, such quick capacitance loss within iodide-based electrolytes is associated with the formation of solid-state deposits of polyiodides at the electrode/electrolyte interface, usually leading to blockage of electrode porosity [50]. Consequently, the redundant polyiodides gradually reduced the number of active sites within porous texture available for the redox reaction. Interestingly, despite the iodide/iodonium salt interactions there could still be a formation of polyiodides from electrolyte ions affecting the cycle-life of a device. Migration of iodides/polyiodides towards negative electrode could be another reason for the EC capacitance fade. It is important to note that, in the case of the cell with 1 M Li_2SO_4, we did not observe such behaviour. It means that the unwanted formation of the polyiodides was restricted/prohibited as there were no free I^- ions present at the positive electrode interface. Therefore, the iodonium salt was effectively used as an electrode dopant, providing capacitance improvement over cycle life of a device. Long-term cycling of CNTs◦I (Fig. 7) shows that incorporated iodonium salts in the electrode material is very stable, and does not follow side reactions so easily, contrary to the free iodide anion from the electrolyte. Thus, operation with Li_2SO_4 is boosted by a redox activity $I_2/2I^-$ attached to the SWCNTs, ensuring good longevity of the system with high capacitance and good process efficiency.

Fig. 8 presents Ragone plot of the cells assembled with different electrolytes showing comparable values of specific energy and power (7.1 Wh kg^{-1} with 315 W kg^{-1} for 1 M Li_2SO_4 and 13.5 Wh kg^{-1} with 240 W kg^{-1} for 1 M KI) to the values that can be found in the literature

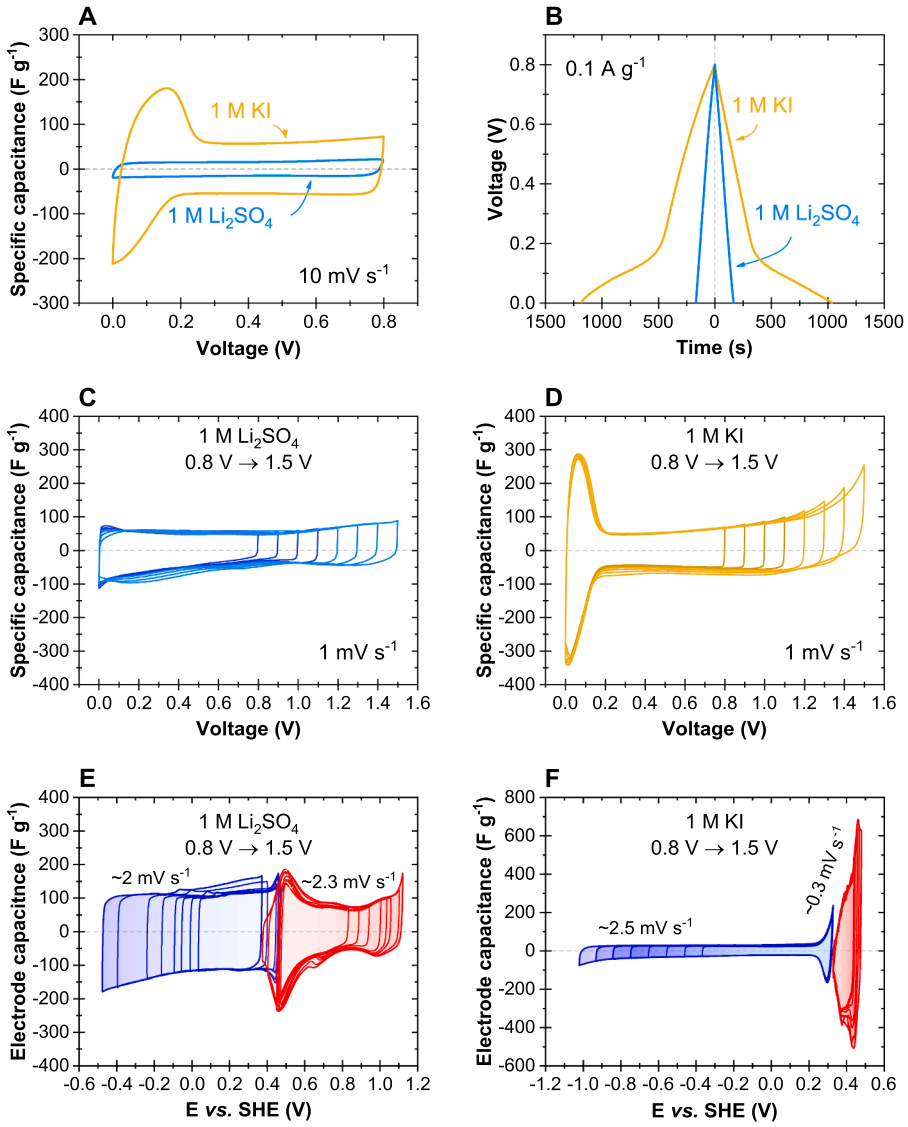

Fig. 5. A) Comparison of electrochemical behaviour of (-) Kynol ‖ CNTs∘I (+) assembled with 1 M Li_2SO_4 and 1 M KI. Cyclic voltammogram at 10 mV s^{-1}, B) Galvanostatic charge/discharge at 0.1 A $g^{-1,}$ C) Voltage window extension at 1 mV s^{-1} in 1 M Li_2SO_4, D) Voltage extension window at 1 mV s^{-1} in 1 M KI, E) Electrodes operation during potential extension in 1 M Li_2SO_4, and F) Electrodes behaviour during potential extension in 1 M KI.

for systems using iodides as an electrolyte [23].

4. Conclusions

Self-standing films from single-walled carbon nanotubes (CNTs) were doped with iodonium salt, i.e., pyridine iodine monochloride (IPyCl or I), and for the first time utilized in electrochemical capacitors. The nanotubular carbon material was pure and, free of defects, and hence highly electrically conducting, making it an excellent choice for the application as electrodes. Moreover, the addition of the iodonium salt improved the electrical conductivity of CNTs four-fold, further increasing the potential of this material for electrochemical applications. CNTs doped with iodonium salt (CNTs∘I) were then used to assemble an asymmetric device with activated carbon cloth as a negative electrode. Neutral 1 M Li_2SO_4 and redox 1 M KI electrolytes were used as electrolytes. In both cases, the positive electrode was the source of redox reactions, which were substantially boosted by the presence of iodonium salt. Interestingly, in the system with 1 M Li_2SO_4, the presence of a redox reaction within the typical region for iodides was observed. It indicated that the iodonium salt did not only enhanced the conductivity of CNTs, but also improved the capacitance by incorporation of redox reaction. It is also essential to mention that, to our surprise, the inclusion of the iodonium salt prevented the surface of CNTs from oxidation, increasing their utility for electrochemistry.

The system assembled with 1 M KI showed a huge improvement in capacitance caused by the presence of redox characteristic for iodides. Interestingly, when doped CNTs were used as an electrode material, the electrochemical behaviour changed, indicating interactions between iodonium salt and iodides dissolved in the electrolyte. The sulphate based system showed 25 F g^{-1} at 0.1 A g^{-1} in the range of 1.5 V, while the system containing iodides exhibited 68 F g^{-1} at 0.1 A g^{-1} in the range of 1.2 V. Such difference in reachable capacitance for both systems could indicate the crucial role of the formation of polyiodides in the system employing 1 M KI.

The assembled cells were also subjected to the assessment of their cycle-life at 1 A g^{-1}. The system's capacitance with 1 M Li_2SO_4 was maintained above 80% of initial capacitance over as many as 10 000 cycles. It is also the first time when CNTs were used as a positive electrode in ECs at such an elevated voltage (1.5 V). The long-term stability of (CNTs∘I) confirmed that deposited iodonium salt protected the surface of the CNTs from oxidation. The system with 1 M KI showed typical capacitance fade related to the formation of polyiodides, their

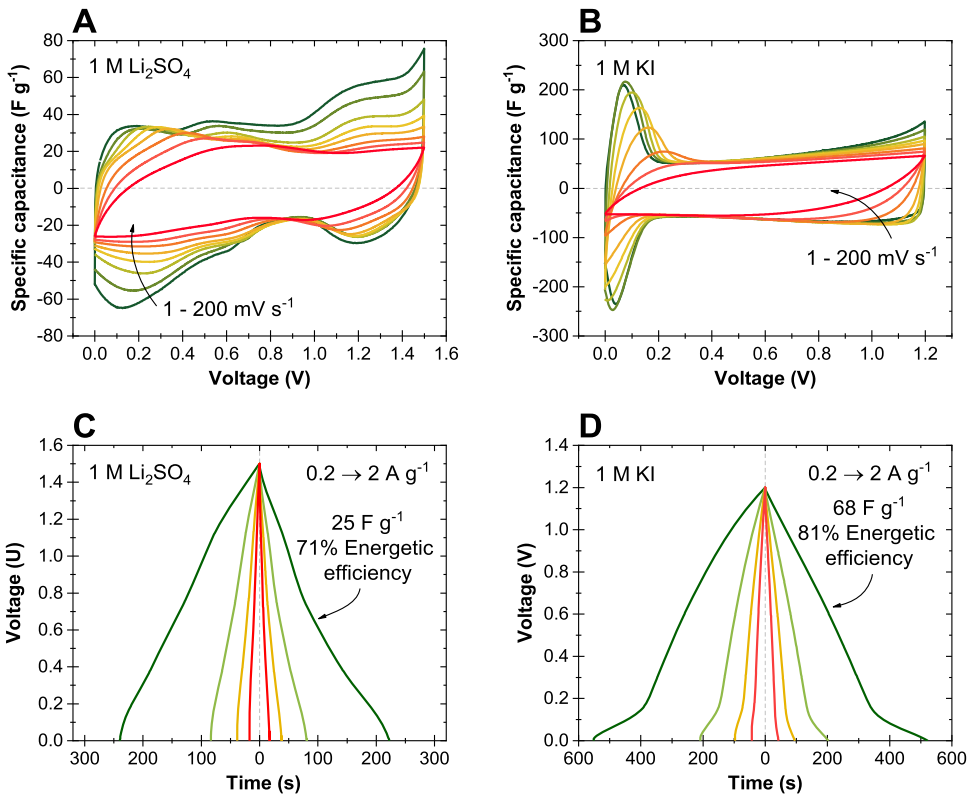

Fig. 6. Electrochemical tests for system (-) Kynol ‖ CNTs∘I (+). Cyclic voltammograms at different scan rates (1 – 200 mV s^{-1}), (A) 1 M Li_2SO_4 and (B) 1 M KI. Charge/discharge at different current densities (0.2 – 2 A g^{-1}), (C) 1 M Li_2SO_4, (D) 1 M KI.

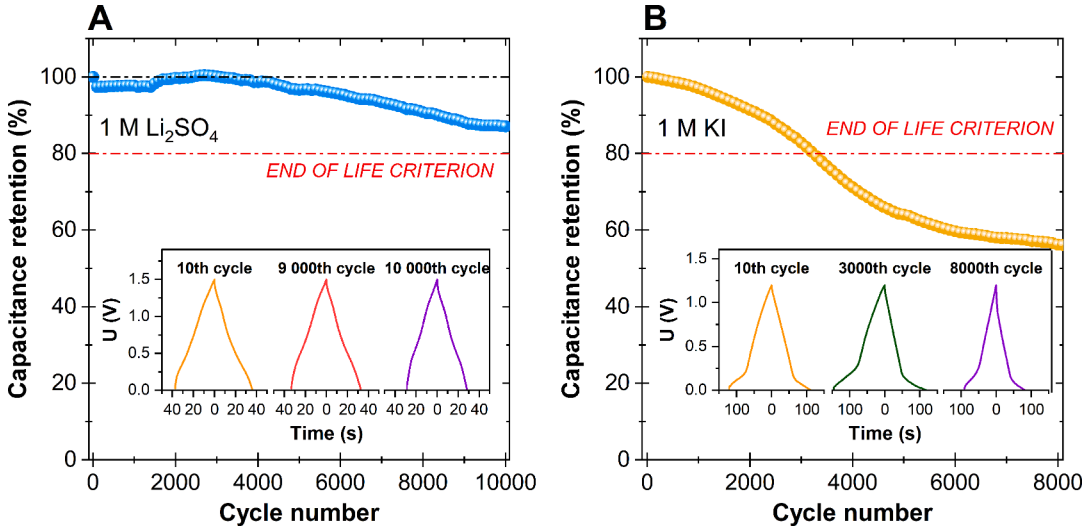

Fig. 7. Cycle-life test of (-) Kynol ‖ CNTs∘I (+) cells assembled with (A) 1 M Li_2SO_4, and (B) 1 M KI. Both cells were cycled at 1 A g^{-1} within the given voltage range until 10 000 cycles.

immobilization within electrode texture, and consequent cyclic ability failure. To sum up, the use of iodonium salt as a dopant can effectively improve the specific capacitance of the ECs by incorporating redox reactions and also provide long-term and stable electrochemical performance in neutral electrolytes.

CRediT authorship contribution statement

Maciej Tobis: Writing – original draft, Methodology, Investigation, Formal analysis, Data curation, Conceptualization. **Justyna Piwek:** Methodology, Investigation. **Anetta Płatek-Mielczarek:** Methodology, Investigation. **Łukasz Przypis:** Methodology, Investigation. **Dawid Janas:** Writing – review & editing, Supervision, Methodology, Investigation, Conceptualization. **Elżbieta Frąckowiak:** Writing – review & editing, Supervision, Resources, Conceptualization.

Declaration of competing interest

The authors declare that they have no known competing financial interests or personal relationships that could have appeared to influence

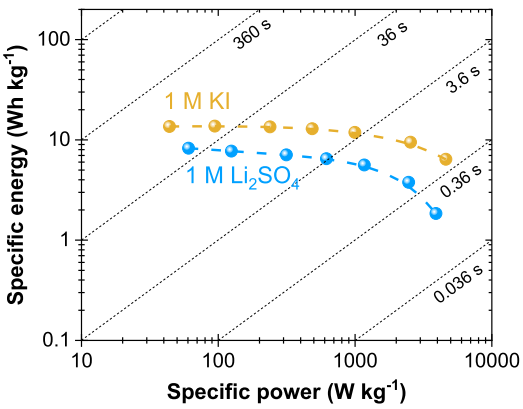

Fig. 8. Ragone plot for ECs consisting of (-) Kynol ‖ CNTs∘I (+) assembled with 1 M KI operating at 1.2 V and 1 M Li_2SO_4 working at 1.5 V.

the work reported in this paper.

Data availability

Data will be made available on request.

Acknowledgements

The authors would like to acknowledge project 0911/SBAD/2401 for financial support.

Supplementary materials

Supplementary material associated with this article can be found, in the online version, at doi:10.1016/j.electacta.2024.144386.

References

[1] M. Lu, F. Beguin, E. Frackowiak, Supercapacitors: Materials, Systems, and Applications, John Wiley & Sons, 2013. Incorporated.
[2] P. Simon, Y. Gogotsi, Materials for electrochemical capacitors, Nat. Mater. 7 (2008) 845–854, https://doi.org/10.1038/nmat2297.
[3] J.R. Miller, P. Simon, Materials science. Electrochemical capacitors for energy management, Science 321 (2008) 651–652, https://doi.org/10.1126/science.1158736.
[4] P. Galek, A. Mackowiak, P. Bujewska, K. Fic, Three-dimensional architectures in electrochemical capacitor applications - insights, opinions, and perspectives, Front. Energy Res. 8 (2020), https://doi.org/10.3389/fenrg.2020.00139.
[5] M.P. Down, S.J. Rowley-Neale, G.C. Smith, C.E. Banks, F.abrication of graphene oxide supercapacitor devices, ACS Appl. Energy Mater. 1 (2018) 707–714, https://doi.org/10.1021/acsaem.7b00164.
[6] P. Ratajczak, M.E. Suss, K. Kaasik, B. Beguin, Carbon electrodes for capacitive technologies, Energy Storage Mater. 16 (2019) 126–145, https://doi.org/10.1016/j.ensm.2018.04.031.
[7] E. Frackowiak, M. Foroutan Koudahi, M. Tobis, Electrochemical capacitor performance of nanotextured carbon/transition metal dichalcogenides composites, Small 17 (2021) 2170255, https://doi.org/10.1002/smll.202170255.
[8] J. Xu, K. Wang, S.Z. Zu, B.H. Han, Z. Wei, Hierarchical nanocomposites of polyaniline nanowire arrays on graphene oxide sheets with synergistic effect for energy storage, ACS Nano 4 (2010) 5019–5026, https://doi.org/10.1021/nn1006539.
[9] A. Sajedi-Moghaddam, C.C. Mayorga-Martinez, E. Saievar-Iranizad, Z. Sofer, M. Pumera, Exfoliated transition metal dichalcogenide (MX_2; M=Mo, W; X=S, Se, Te) nanosheets and their composites with polyaniline nanofibers for electrochemical capacitors, Appl. Mater. Today 16 (2019) 280–289, https://doi.org/10.1016/j.apmt.2019.06.002.
[10] R. Wang, et al., Fast proton insertion in layered $H_2W_2O_7$ via selective etching of an aurivillius phase, Adv. Energy Mater. 11 (2021) 2003335, https://doi.org/10.1002/aenm.202003335.
[11] J.B. Mitchell, et al., Confined interlayer water promotes structural stability for high-rate electrochemical proton intercalation in tungsten oxide hydrates, ACS Energy Lett. 4 (2019) 2805–2812, https://doi.org/10.1021/acsenergylett.9b02040.
[12] A. Slesinski, S. Sroka, K. Fic, E. Frackowiak, J. Menzel, Operando monitoring of local pH value changes at the carbon electrode surface in neutral sulfate-based aqueous electrochemical capacitors, ACS Appl. Mater. Interfaces 14 (2022) 37782–37792, https://doi.org/10.1021/acsami.2c09920.
[13] A. Platek-Mielczarek, C. Nita, C. Matei Ghimbeu, E. Frackowiak, K. Fic, Link between alkali metals in salt templates and in electrolytes for improved carbon-based electrochemical capacitors, ACS Appl. Mater. Interfaces 13 (2021) 2584–2599, https://doi.org/10.1021/acsami.0c18627.
[14] F. Béguin, V. Presser, A. Balducci, E. Frackowiak, Carbons and electrolytes for advanced supercapacitors, Adv. Mater. 26 (2014) 2219–2251, https://doi.org/10.1002/adma.201304137.
[15] E. Frackowiak, F. Béguin, Electrochemical storage of energy in carbon nanotubes and nanostructured carbons, Carbon 40 (2002) 1775–1787, https://doi.org/10.1016/S0008-6223(02)00045-3.
[16] D. Aradilla, et al., High performance of symmetric micro-supercapacitors based on silicon nanowires using N-methyl-N-propylpyrrolidinium bis (trifluoromethylsulfonyl)imide as electrolyte, Nano Energy 9 (2014) 273–281, https://doi.org/10.1016/j.nanoen.2014.07.001.
[17] E. Frackowiak, F. Béguin, Carbon materials for the electrochemical storage of energy in capacitors, Carbon 39 (2001) 937–950, https://doi.org/10.1016/S0008-6223(00)00183-4.
[18] D. Janas, A.P. Herman, S. Boncel, K.K.K. Koziol, Iodine monochloride as a powerful enhancer of electrical conductivity of carbon nanotube wires, Carbon 73 (2014) 225–233, https://doi.org/10.1016/j.carbon.2014.02.058 (New York).
[19] C. Niu, E.K. Sichel, R. Hoch, D. Moy, H. Tennent, High power electrochemical capacitors based on carbon nanotube electrodes, Appl. Phys. Lett. 70 (1997) 1480–1482, https://doi.org/10.1063/1.118568.
[20] E. Frackowiak, K. Jurewicz, S. Delpeux, F. Béguin, Nanotubular materials for supercapacitors, J. Power Sources 97 (2001) 822–825, https://doi.org/10.1016/S0378-7753(01)00736-4.
[21] M.S. Dresselhaus, G. Dresselhaus, P.C. Eklund, Science of Fullerenes and Carbon Nanotubes: Their Properties and Applications, Elsevier Science & Technology, 1996.
[22] K. Fic, S. Morimoto, E. Frąckowiak, M. Ishikawa, Redox activity of bromides in carbon-based electrochemical capacitors, Batter. Supercaps 3 (2020) 1080–1090, https://doi.org/10.1002/batt.202000061.
[23] P. Przygocki, Q. Abbas, F. Béguin, Capacitance enhancement of hybrid electrochemical capacitor with asymmetric carbon electrodes configuration in neutral aqueous electrolyte, Electrochim. Acta 269 (2018) 640–648, https://doi.org/10.1016/j.electacta.2018.03.016.
[24] H. Fitzek, et al., Impact of iodine electrodeposition on nanoporous carbon electrode determined by EQCM, XPS and *in situ* Raman spectroscopy, Nanomaterials 13 (2023) 1545, https://doi.org/10.3390/nano13091545.
[25] G. Lota, E. Frackowiak, Striking capacitance of carbon/iodide interface, Electrochem. Commun. 11 (2009) 87–90, https://doi.org/10.1016/j.elecom.2008.10.026.
[26] G. Lota, K. Fic, E. Frackowiak, Alkali metal iodide/carbon interface as a source of pseudocapacitance, Electrochem. Commun. 13 (2011) 38–41, https://doi.org/10.1016/j.elecom.2010.11.007.
[27] E. Frackowiak, M. Meller, J. Menzel, D. Gastol, K. Fic, Redox-active electrolyte for supercapacitor application, Faraday Discuss. 172 (2014) 179–198, https://doi.org/10.1039/c4fd00052h.
[28] P. Przygocki, Q. Abbas, P. Babuchowska, F. Béguin, Confinement of iodides in carbon porosity to prevent from positive electrode oxidation in high voltage aqueous hybrid electrochemical capacitors, Carbon 125 (2017) 391–400, https://doi.org/10.1016/j.carbon.2017.09.060.
[29] C. Prehal, et al., Persistent and reversible solid iodine electrodeposition in nanoporous carbons, Nat. Commun. 11 (2020) 4838, https://doi.org/10.1038/s41467-020-18610-6.
[30] P. Barpanda, G. Fanchini, G.G. Amatucci, The physical and electrochemical characterization of vapor phase iodated activated carbons, Electrochim. Acta 52 (2007) 7136–7147, https://doi.org/10.1016/j.electacta.2007.05.051.
[31] G. Lota, et al., The modified activated carbon treated with a low-temperature iodine plasma used as electrode material for electrochemical capacitors, Mater. Lett. 175 (2016) 96–100, https://doi.org/10.1016/j.matlet.2016.04.040.
[32] P. Taborowska, et al., Doping of carbon nanotubes by halogenated solvents, Sci. Rep. 12 (2022) 7004, https://doi.org/10.1038/s41598-022-11162-3.
[33] B.M. Maciejewska, M. Jasiurkowska-Delaporte, A.I. Vasylenko, K.K. Kozioł, S. Jurga, Experimental and theoretical studies on the mechanism for chemical oxidation of multiwalled carbon nanotubes, RSC Adv. 4 (2014) 28826–28831, https://doi.org/10.1039/C4RA03881A.
[34] J.S. Bulmer, A. Lekawa-Raus, D.G. Rickel, F.F. Balakirev, K.K. Koziol, Extreme magneto-transport of bulk carbon nanotubes in sorted electronic concentrations and aligned high performance fiber, Sci. Rep. 7 (2017) 12193, https://doi.org/10.1038/s41598-017-12546-6. -12113.
[35] X. Zhang, W. Lu, G. Zhou, Q. Li, Understanding the mechanical and conductive properties of carbon nanotube fibers for smart electronics, Adv. Mater. 32 (2020) 1902028, https://doi.org/10.1002/adma.201902028.
[36] B. Kumanek, et al., Doping engineering of single-walled carbon nanotubes by nitrogen compounds using basicity and alignment, ACS Appl. Mater. Interfaces 14 (2022) 25861–25877, https://doi.org/10.1021/acsami.2c00970.
[37] D. Janas, K.Z. Milowska, P.D. Bristowe, K.K.K. Koziol, Improving the electrical properties of carbon nanotubes with interhalogen compounds, Nanoscale 9 (2017) 3212–3221, https://doi.org/10.1039/c7nr00224f.
[38] S.D.M. Brown, A. Jorio, P. Corio, M.S. Dresselhaus, G. Dresselhaus, R. Saito, K. Kneipp, Origin of the Breit-Wigner-Fano lineshape of the tangential G-band feature of metallic carbon nanotubes, Phys. Rev. B 63 (2001), https://doi.org/10.1103/PhysRevB.63.155414.

[39] R. Yang, Z. Shi, L. Zhang, D. Shi, G. Zhang, Observation of Raman G-peak split for graphene nanoribbons with hydrogen-terminated Zigzag edges, Nano Lett. 11 (2011) 4083–4088, https://doi.org/10.1021/nl201387x.
[40] S. Ghosh, S.R.K.C.S. Yamijala, S.K. Pati, C.N.R. Rao, The interaction of halogen molecules with SWNTs and graphene, RSC Adv. 2 (2012) 1181–1188, https://doi.org/10.1039/C1RA00295C.
[41] T. Kupka, M. Stachów, L. Stobiński, J. Kaminský, Calculation of Raman parameters of real-size zigzag (n, 0) single-walled carbon nanotubes using finite-size models, Phys. Chem. Chem. Phys. 18 (2016) 25058–25069, https://doi.org/10.1039/C6CP04100K.
[42] P.C. Eklund, A.M. Rao, S. Bandow, A. Thess, R.E. Smalley, Evidence for charge transfer in doped carbon nanotube bundles from Raman scattering, Nature 388 (1997) 257–259, https://doi.org/10.1038/40827.
[43] B. Kumanek, et al., Convenient but powerful method to dope single-walled carbon nanotube films with iodonium salts, Appl. Nanosci. 10 (2020) 529–539, https://doi.org/10.1007/s13204-019-01133-y.
[44] P. Klaeboe, The Raman spectra of some iodine, bromine, and iodine monochloride charge-transfer coomplexes in solution, J. Am. Chem. Soc. 89 (1967) 3667–3676, https://doi.org/10.1021/ja00991a001.
[45] M. Thommes, et al., Physisorption of gases, with special reference to the evaluation of surface area and pore size distribution (IUPAC Technical Report), Pure Appl. Chem. 87 (2015) 1051–1069, https://doi.org/10.1515/pac-2014-1117.
[46] S.K. Hadjikakou, N. Hadjiliadis, Interaction of thioamides, selenoamides, and amides with diiodine, Bioinorg. Chem. Appl. 2006 (2006) 1–10, https://doi.org/10.1155/BCA/2006/60291.
[47] Y.L. Wang, J.C. Nagy, D.W. Margerum, Kinetics of hydrolysis of iodine monochloride measured by the pulsed-accelerated-flow method, J. Am. Chem. Soc. 111 (1989) 7838–7844, https://doi.org/10.1021/ja00202a026.
[48] A. Peigney, C. Laurent, E. Flahaut, R.R. Bacsa, A. Rousset, Specific surface area of carbon nanotubes and bundles of carbon nanotubes, Carbon 39 (2001) 507–514, https://doi.org/10.1016/S0008-6223(00)00155-X.
[49] S. Chakraborty, et al., Surface area measurement of functionalized single-walled carbon nanotubes, J. Phys. Chem. B 110 (2006) 24812–24815, https://doi.org/10.1021/jp065044u.
[50] A. Platek, J. Piwek, K. Fic, E. Frackowiak, Ageing mechanisms in electrochemical capacitors with aqueous redox-active electrolytes, Electrochim. Acta 311 (2019) 211–220, https://doi.org/10.1016/j.electacta.2019.04.117.
[51] Q. Abbas, H. Fitzek, H. Schröttner, S. Dsoke, B. Gollas, Immobilization of polyiodide redox species in porous carbon for battery-like electrodes in eco-friendly hybrid electrochemical capacitors, Nanomaterials 9 (2019) 1413, https://doi.org/10.3390/nano9101413.
[52] A. Burke, M. Miller, Testing of electrochemical capacitors: capacitance, resistance, energy density, and power capability, Electrochim. Acta 55 (2010) 7538–7548, https://doi.org/10.1016/j.electacta.2010.04.074.